

Accepted Manuscript

Title: Effect of Sn additives on the CuZnAl–HZSM-5 hybrid catalysts for the direct DME synthesis from syngas

Author: M. Cai V. Subramanian V.V. Sushkevich V.V. Ordonsky A.Y. Khodakov



PII: S0926-860X(15)30046-6
DOI: <http://dx.doi.org/doi:10.1016/j.apcata.2015.06.030>
Reference: APCATA 15442

To appear in: *Applied Catalysis A: General*

Received date: 24-3-2015
Revised date: 19-6-2015
Accepted date: 22-6-2015

Please cite this article as: M.Cai, V.Subramanian, V.V.Sushkevich, V.V.Ordonsky, A.Y.Khodakov, Effect of Sn additives on the CuZnAlndashHZSM-5 hybrid catalysts for the direct DME synthesis from syngas, Applied Catalysis A, General <http://dx.doi.org/10.1016/j.apcata.2015.06.030>

This is a PDF file of an unedited manuscript that has been accepted for publication. As a service to our customers we are providing this early version of the manuscript. The manuscript will undergo copyediting, typesetting, and review of the resulting proof before it is published in its final form. Please note that during the production process errors may be discovered which could affect the content, and all legal disclaimers that apply to the journal pertain.

Effect of Sn additives on the CuZnAl-HZSM-5 hybrid catalysts for the direct DME synthesis from syngas

M. Cai^a, V. Subramanian^a, V.V. Sushkevich^b, V.V. Ordonsky^{a*}, A. Y. Khodakov^{a*},

^a*Unité de catalyse et de chimie du solide (UMR 8181 CNRS), Université Lille 1-ENSCL-EC Lille, Bat. C3, Cité Scientifique, 59655 Villeneuve d'Ascq, France*

^b*Department of Chemistry, Lomonosov Moscow State University, Leninskye Gory 1/3, 119991 Moscow, Russia*

Highlights

► Tin-promoted Cu-Zn-Al/HZSM-5 catalysts were studied in dimethyl ether synthesis ► Presence of tin in reduced state leads to modification of electronic state of Cu ► Tin suppresses the WGS reaction and consequently reduces CO₂ production ► The effect is due to the deactivation of positively charged Cu species active in WGS ► Further increase of tin loading leads to decrease of carbon monoxide conversion

Abstract

Tin-promoted bifunctional Cu-Zn-Al/HZSM-5 catalysts were prepared in order to increase the selectivity of carbon monoxide hydrogenation to dimethyl ether (DME). The catalysts were characterized by H₂-TPR, in-situ XRD, XPS, in-situ XANES and FTIR. The characterization revealed that the electronic properties and surface distribution of Cu in the catalysts were significantly changed by tin addition leading to the decrease in the fraction of ionic Cu species (Cu⁺ and Cu²⁺) and positively charged metallic Cu^{δ+} sites. Addition of tin suppressed the water gas shift reaction and decreases the selectivity to undesirable CO₂. As a result, the selectivity to valuable DME and methanol increased for the mildly promoted catalysts. Further increase in Sn loading led to the decrease in the overall rate of carbon monoxide conversion.

Keywords: Selective poisoning; tin; CuO-ZnO-Al₂O₃ catalyst; DME synthesis

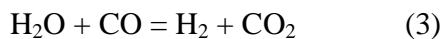
*Corresponding authors: E-mail address: vitaly.ordomsky@univ-lille1.fr (V.V. Ordonsky); andrei.khodakov@univ-lille1.fr (A.Y. Khodakov)

1. Introduction

Recently, research toward alternative energy has triggered considerable attention due to the depletion of oil resources and environmental concerns [1]. To meet the future demand, utilization of the alternative energy feedstocks such as natural gas, coal and biomass could be extremely important. These alternative feedstocks can be converted via steam reforming, partial oxidation or gasification into syngas (H_2/CO mixture) which is a valuable intermediate for manufacturing fuels and chemicals [2–5].

Conversion of syngas to dimethyl ether (DME) has attracted immense interest due to the merits of DME: (i) an attractive alternative to the diesel due to its low NO_x , CO emission and high cetane number, (ii) chemical feedstock for the synthesis of dimethyl sulfate, methyl acetate and lower olefins, (iii) LPG substitute and hydrogen source for fuel cell applications [6–8]. DME is conventionally prepared by dehydration of methanol over acid catalysts (zeolites, $\gamma-Al_2O_3$) [9–11]. In the indirect DME synthesis, methanol is first synthesized from syngas using mainly Cu-ZnO based catalysts. The single pass conversion in methanol synthesis is low and limited by thermodynamics. Methanol is then dehydrated to DME at the second stage.

Direct DME synthesis from syngas overcomes thermodynamic limitations and could result in higher DME production rates. The direct DME synthesis from syngas is usually composed of three reaction steps: hydrogenation of CO to methanol, methanol dehydration to DME and water-gas-shift reaction (WGSR). The relevant chemical equations (1)-(3) are shown below:



The combination of reactions (1)–(3) gives the overall equation:



The bifunctional catalyst for direct DME synthesis from syngas contains two major components: a methanol synthesis catalyst and a methanol dehydration catalyst [12]. A high degree of intimacy and synergism between these components is extremely important to get the enhanced catalytic performance. The copper based catalyst for methanol synthesis is mature in terms of understanding its preparation, catalytic performance and reaction conditions [13, 14]. Hence, considerable attention has been recently paid toward the research on the dehydration component and optimization of its preparation and mixing with the methanol synthesis catalyst [15–17]. The research conducted so far suggests that a moderate acidity is required for effective dehydration step in order to avoid lower DME selectivity because of hydrocarbon formation.

During the direct synthesis of DME, the reactions mentioned in Eq (1) and Eq (3) are catalyzed by the methanol synthesis catalyst. It is also known that copper based catalysts exhibit high activity in water gas shift reaction, which could result in the ample amount of CO_2 . Most of previous works have addressed either optimization of overall activity of bifunctional catalysts for direct DME synthesis or lowering hydrocarbon production, while very few reports have focused on reducing carbon dioxide selectivity. Thus, Sun et al. [18] studied the effect of addition of different amounts of ZrO_2 in $\text{CuO}/\text{ZnO}/\text{ZrO}_2/\text{HZSM-5}$ instead of commonly used alumina. The authors explained the increase in the activity and selectivity of the catalyst to DME by Cu^+ species stabilized by ZrO_2 in the presence of metallic Cu. Moreover, a study reported by Li et al. [19] gave similar results about addition of La_2O_3 promoter with better catalytic performance

compared with Cu-ZrO₂/γ-Al₂O₃ catalyst in CO conversion and enhanced DME selectivity due to the higher dispersion of copper species. Manganese has been also found as effective promoter of the catalyst activity in DME synthesis [20-21]. The authors have explained the effect by formation of Cu-Mn spinel oxide with higher dispersion of metallic copper in the reduced catalyst and higher rate in WGSR. Thus, these works have been more focused on the development of active catalyst usually by increase of the copper surface area.

Note that CO₂ is a major product in this reaction; its production can drastically undermine the carbon efficiency of the whole process. One of the ways to reduce the CO₂ selectivity in direct DME synthesis could be catalyst promotion. It can be expected that the efficient promoter would reduce the rate of WGSR, while the rate of DME synthesis could be only slightly affected.

Tin has been used as a promoter for a number of metal catalysts where it principally affects their hydrogenation activity. There have been numerous studies during the last decade devoted to noble metal hydrogenation catalysts (Pd, Pt, Ru) modified by tin [22-24]. Particularly, the alloys of tin with platinum have been shown to significantly enhance the selectivity of the hydrogenation to the α-β-unsaturated aldehydes. The reason of this catalytic effect is not well understood and different hypotheses exist: Sn might induce electronic effects on Pt, changing its adsorption properties or act a site-blocking agent changing the adsorption site of the molecules. To the best of our knowledge, the effect of tin on Cu hydrogenation catalysts has not been yet addressed in the literature.

The goal of the present work is to reduce the carbon dioxide selectivity in direct DME synthesis from syngas by promotion of CuZnAl-HZSM-5 hybrid catalysts with tin. We suggest that there could be different active species for methanol synthesis and WGSR. Indeed, it has been shown earlier that activity in WGSR correlates with the amount of Cu⁺ sites with low redox potential between Cu⁺ and Cu²⁺ during WGSR [25]. At the same time, the activity in methanol

synthesis correlates usually with surface area of metallic copper in the catalyst [26]. Thus, it might be possible to selectively deactivate the most active positively charged copper sites by electron donation from tin with increase in the selectivity to methanol and DME. A combination of characterization techniques (in-situ XRD, TPR, XPS, in-situ XANES and FTIR) were used to characterize the properties of the promoted catalysts. The catalytic performances in direct DME synthesis and water gas shift reaction were evaluated in a fixed reactor.

2. Experimental

2.1 Catalyst preparation

The CuO–ZnO–Al₂O₃ precursor (Cu:Zn:Al = 60:30:10 atomic ratio) was prepared by coprecipitation at constant pH (ca. 7) and constant temperature (70°C). A solution containing metal nitrates ($[\text{Cu}^{2+}] + [\text{Zn}^{2+}] + [\text{Al}^{3+}] = 1.0 \text{ M}$) and a sodium carbonate solution (1.0 M) were simultaneously added to a reaction vessel containing 10 mL of deionized water. The suspension was continuously stirred and kept at the desired pH by adjustment of the relative flow rates of the two solutions. The final suspension was aged under stirring at 70°C for 1 h. The precipitate was filtered off, repeatedly washed with sufficient deionized water to remove residual sodium ions, dried at 110°C overnight and then finally calcined at 350°C in flowing air for 6 h yielding the Cu–Zn–Al (CZA) catalyst.

The xSn-CZA catalysts were prepared by sequential impregnation using incipient wetness method at different Sn loading, 0.1, 0.2, 0.5 and 1.0 wt. %, respectively. After the impregnation with a SnCl₂ solution, the promoted catalysts were dried at 90°C for 12 h followed by calcination in air at 360 °C for 5 h.

The HZSM-5 zeolite was prepared by calcination of $\text{NH}_4\text{-ZSM-5}$ (Zeolyst CBV2314, $\text{SiO}_2/\text{Al}_2\text{O}_3 = 23$) in tubular furnace under the flow of air at 550°C for 6 h (at the heating rate of $2^\circ\text{C}/\text{min}$).

The hybrid catalysts were prepared by physically mixing of the powders (under 150 mesh) of the prepared CZA catalyst and zeolite (5:3 wt/wt, 1:1 wt/wt, or 1/2 wt/wt), pressing the mixture into tablets and finally crushing them into fractions before reaction.

2.2 Characterizations

NH_3 -TPD profiles were obtained in an Autochem 2910 equipment (Micromeritics) coupled with a quadrupole mass spectrometer (OmniStar from Balzers Instruments). Prior to ammonia adsorption, ca. 100 mg of sample was pretreated at 500°C for 60 min in He. Subsequently, calibrated pulses of NH_3 were introduced at 50°C until saturation of the sample. The chemisorbed ammonia was then desorbed by heating from 50°C to 1000°C at a heating rate of $10^\circ\text{C}/\text{min}$. The $m/z = 16$ signal in the coupled mass spectrometer was used to obtain the corresponding NH_3 desorption profiles.

The temperature-programmed reduction (TPR) profiles were obtained by passing 10% H_2/Ar gas mixture through the catalyst while increasing the temperature at a linear rate. 100 mg of the samples were loaded into a quartz reactor and pretreated by a He flow (30 ml/min STP) at 100°C for 2 h. Then He was replaced by the reductive gas H_2/He (5 mol% H_2 in He) at the same flow-rate of 30 ml/min. The temperature was increased up to 800°C at a ramp rate of $5^\circ\text{C}/\text{min}$. The effluent gas was analysed by a thermal conductivity detector (TCD).

Copper surface area and dispersion were measured using a N_2O decomposition method. The catalysts (100 mg) were first reduced upon heating to 290°C in a 10% H_2/Ar mixture (40 mL/min) with a ramp of $5^\circ\text{C}/\text{min}$, and the temperature was maintained for 2 h. The amount of hydrogen consumed is denoted as n_1 . Then, the reduced samples were cooled to 50°C and purged

with Ar for 30 min. The samples were exposed to 10% N₂O/Ar for 1 h to oxidize surface copper to Cu₂O and then flushed with Ar to remove the N₂O. Finally, TPR was performed under a 10% H₂/Ar flow to reduce Cu₂O back to metallic Cu using a ramp rate of 5°C/min to 300°C. The amount of H₂ consumed is denoted as n_2 . The Cu dispersion and exposed Cu surface area of the catalysts were calculated as:

$$D_{Cu} = \frac{2 \cdot n_2}{n_1} \times 100\% ;$$

$$S_{Cu} = \frac{2 \cdot n_2 \cdot N}{1.4 \cdot 10^{19}}$$

where D_{Cu} (%) is the dispersion of Cu, S_{Cu} (m²/g) is the exposed copper surface area per gram of the catalyst, N is the Avogadro's constant (6.02×10^{23} atoms/mol), and (1.4×10^{19}) is the number of copper atoms per square meter.

The crystal structure of the catalysts were revealed by X-ray diffraction (XRD) on a Bruker D8 Advance diffractometer, using CuK α radiation ($\lambda = 1.5406 \text{ \AA}$) as X-ray source. A $10^\circ < 2\theta < 80^\circ$ range was scanned with step of 0.02°/s and the 2 s acquisition time.

X-ray photoelectron spectra (XPS) were acquired on a Kratos Axis Ultra DLD apparatus equipped with a hemispherical analyses and a delay line detector on calcined powder samples and after in situ reduction (at 290°C for 6 h for the CZA catalysts). The reduction was carried out in the atmospheric pressure reaction cell attached to the preparation chamber of the spectrometer with a heating rate of 2°C/min like during reaction. The experiments were performed using an Al monochromatized X-ray source (10 kV, 15 mA) with a pass energy of 40 eV (0.1 eV/step) for high resolution spectra and a pass energy of 160 eV (1 eV/step) for the survey spectrum in hybrid

mode and slot lens mode respectively. The binding energies were referenced to the Al 2p core level (74.6 eV).

The in situ time-resolved XRD ($\lambda=0.5 \text{ \AA}$) and XAS data were measured at the BM01B beamline (ESRF, France). For better comparison with the ex-situ XRD results, the diffraction angles in the in-situ XRD patterns were recalculated for the Cu K α X-ray source ($\lambda = 1.5406 \text{ \AA}$). 5–10 mg of catalyst was loaded in the quartz capillary reactor (OD=1 mm, wall thickness = 0.020 mm) and pressed from both sides with quartz wool. A Cyberstar gas blower was used to control the reactor temperature. A gas manifold system and a capillary reactor are described elsewhere [27-28]. All the catalyst samples were reduced in situ under flow of pure H₂ (P = 1 bar) during the temperature ramping (3°C/min) up to 290°C and then cooled down to 40°C in H₂ flow. In situ XAS spectra at Cu K-edge were acquired in transmission mode. XRD patterns were acquired using a monochromatic X-ray beam (Si 111 channel-cut monochromator) and a high-resolution diffractometer. The Scherrer equation has been used for the calculation of sizes of CuO and Cu crystallites by analysis of the (002) and (111) reflections in XRD profiles, respectively.

FTIR measurements are carried out on a Nicolet Protege 380 spectrometer equipped with a DTGS detector. Before the measurements all samples were diluted with calcined silica (1:3 by weight) to avoid the full adsorption of IR beam by the catalyst. About 20 mg of the samples were pressed in self-supported wafer. The sample was then introduced in a glass cells specially designed for in-situ FTIR spectroscopy at low temperature (-140°C) and enabling preliminary thermal treatments. The activation procedure started with a heating step (5°C/min) under a vacuum from ambient temperature to 290°C with a 3 h plateau in atmosphere of hydrogen with subsequent evacuation. When the activation procedure was completed, the sample was cooled down to -140°C. Carbon monoxide was then gradually introduced into the cell and IR spectra subsequently recorded. The procedure was repeated until the evolution of adsorbed species

indicated that CO saturation of the surface was reached. Difference spectra were obtained by the subtraction of the reference spectra from the spectra of the samples with adsorbed CO.

2.3 Catalyst reaction

The DME synthesis reaction was carried out in a fixed-bed stainless-steel tubular reactor ($d_{\text{int}} = 8$ mm) operating at high pressure. The catalyst was crushed and sieved to obtain catalyst grains of 63–200 μm in diameter. The catalyst loading was typically 0.5 g. Before reaction, the samples were reduced in hydrogen flow with the flow rate of 30 ml/min. The temperature was increased to 290°C with a heating rate of 2°C/min and then kept at this temperature for 6 h. The thermocouple was in direct contact with the catalyst, so that the thermocouple measurements could reflect the temperature inside the reactor. No temperature spike and temperature swings were observed during the whole catalytic testing. After reduction, the gas flow was switched to premix the syngas with H_2/CO molar ratio of 2/1. The reaction was carried out at 260°C under a pressure of 20 bar maintained using a back pressure regulator, and the gas hourly space velocity (GHSV) of 3600 ml/(g·h). All experimental data were obtained under the steady-state conditions that were usually maintained at least for 3 h. Carbon monoxide gas contained 5% nitrogen, which was used as an internal standard for the conversion and selectivity calculation. The products were sampled from the high pressure side and analysed using an online gas chromatograph with TCD (H_2 , CO, CO_2 and CH_4) and FID (MeOH, DME and other hydrocarbons) detectors. The CO conversions and product selectivities were calculated on carbon basis.

WGSR was carried out at the temperature range of 260°C and atmospheric pressure in a continuous fixed-bed reactor packed with 0.5 g of the Cu-based catalyst. Prior to each experiment, the catalyst was reduced for 6 h at 290°C in an H_2 flow of 30 ml/min. Then He saturated by pure water (0.01 ml/min water in 20 ml/min He) was used as a feed with the space velocity (GHSV) of 3600 ml/(g·h). Moreover, CO with the flow rate of 10 ml/min was

introduced to the reactor for the water gas shift reaction. The performance of the catalysts was measured after 2 h time on stream (TOS) for each experiment. The analysis of the reaction products was carried out on-line using a gas chromatograph equipped with a TCD detector. In the reproducibility tests, the absolute variation of CO conversion and DME selectivity were respectively, less than 5 % and 0.5 %.

The carbon monoxide contained 5% of helium, which was used as an internal standard for calculating carbon monoxide conversion:

$$X_{CO} = \frac{n_{CO}^{in} - n_{CO}^{out}}{n_{CO}^{in}} \times 100\% ;$$

The product selectivity (S) was reported on carbon basis:

$$S_j = \frac{k_C n_j}{n_{CO}^{in} - n_{CO}^{out}} \times 100\% ,$$

where n_{CO}^{in} , n_{CO}^{out} is the mole flow rate of CO in and out of the reactor; n_j is the mole flow rate of formed product; k_C – number of carbon atoms in the product.

3. Results and discussion

3.1 Catalyst characterization

The ZSM-5 zeolite used for the preparation of hybrid catalysts has uniform particle size distribution in the range 5-7 μm (Figure 1a). The zeolite particles consist of agglomerates of intergrown zeolite crystallites. The acidity of materials was studied by TPD NH_3 (Figure 1b). ZSM-5 exhibits the ammonia desorption at two temperatures: a low-temperature peak at 100-300°C and a high-temperature peak at 400-600°C corresponding respectively to the weaker and stronger acid sites. The total amount of acid sites determined by TPD of NH_3 is 993 $\mu\text{mol/g}$. The

aluminum content in the sample determined by ICP analysis is higher (1280 $\mu\text{mol/g}$) due to the fact that a part of aluminum could be in extraframework positions with significantly weaker adsorption of ammonia.

The XRD patterns of calcined CZA catalysts with and without Sn are depicted in Fig. 2. The observed diffraction lines are assigned to CuO and ZnO. The absence of any peaks relevant to Al_2O_3 can be correlated to the amorphous nature of the alumina. Also, no extra peaks corresponding to tin oxide were seen in the XRD patterns. This can be due to low tin content (<1 wt.%) and its high dispersion in matrix CuO-ZnO. Interestingly, tin promotion does not affect the width of CuO and ZnO peaks. Thus, the size of copper and zinc oxide nanoparticles does not change after the tin promotion.

To evaluate the reduction behavior, all the catalysts were analyzed by TPR. The reduction temperature lies between 264 to 280°C (Table 1, Fig. 3). The parent catalyst, without the Sn promotion, showed a lowest reduction temperature of 264°C. An increase in Sn content from 0.1 to 1.0 wt.%, results in higher reduction temperature. The same effect of the promotion with tin was earlier observed in Pt catalysts [29]. The effect has been explained by a reduction of both metals (Pt and Sn) with subsequent alloy formation. Reduction of the parent CZA sample results in the hydrogen consumption (Table 1) similar to the content of CuO in the sample (7.3 $\text{mmol/g}_{\text{cat}}$). This indicates almost total reduction of Cu. Promotion by tin leads to lower hydrogen consumption (Table 1, Fig. 3). This suggests interaction of tin with copper with probable incorporation of tin species into copper oxide and/or possible deposition on the surface of copper oxide with decrease in the catalyst reducibility. Presence of tin in this case might suppress adsorption and migration of hydrogen on the surface with decrease of the rate of copper reduction. N_2O decomposition (Table 1) shows that the surface area of Cu decreases from 36 to 19 m^2/g with the increase in the tin content. The effect can be due to the formation of Cu-Sn

mixed species but without significant segregation of copper with decrease of the amount of active Cu atoms.

To elucidate the change in the surface composition after Sn doping, XPS analysis was performed on the CZA and tin containing catalysts pretreated under both oxidizing and reducing atmospheres. As shown in the Fig. 4a, the Cu 2p_{3/2} binding energy was observed at 933.0 eV and the presence of Cu²⁺ shake up satellite peaks at 942 eV and 962 eV confirms the existence of mainly Cu²⁺ state in the catalysts after oxidation [30]. The XPS spectra of the oxidized catalysts were almost identical. The Cu 2p XPS spectra of xSn-CZA catalysts reduced in H₂ at 290°C are shown in Fig. 4b. The disappearance of satellite peaks and simultaneous shift of the principal Cu 2p_{3/2} peak towards lower binding energies upon H₂-reduction are indicative of copper reduction to Cu⁺ or Cu⁰ [31-32]. XPS indicates almost complete copper reduction. Somewhat lower hydrogen consumption in TPR experiments can be due to autoreduction of non-reduced part of copper oxide into metallic copper at higher temperatures over tin promoted catalysts. The Cu 2p_{3/2} BE values and widths of Cu⁺ and Cu⁰ species are almost identical. These species are difficult to distinguish from the XPS spectra [33]. However, it is interesting to note that the maximum of the peak is slightly shifting for tin treated catalysts in the direction of lower BE (Fig. 4, Table 1). Earlier the shift of the XPS peak to the lower BE has been observed over reduced noble metal catalysts promoted by tin [34] and was explained by charge transfer from Sn to the noble metal due to the formation of alloy with tin. The area of Cu 2p_{3/2} peak decreases with increase in the tin content (Table 1). This could be due to the analysis of only surface species by XPS where content of Cu should be lower due to the presence of tin.

For better clarity, the Sn 3d_{5/2} XPS spectra have been analyzed before and after reduction of the catalysts. The spectra recorded over fresh catalyst (Fig. 5) show a peak about 486.5 eV which might be assigned to the oxidized tin (Sn^{IV} or Sn^{II}) [35]. A new peak appears at 485 eV

after reduction which might be assigned to metallic tin. Thus, the XPS results suggest that tin is partially reduced to metallic state. However, the relative amount of metallic tin seems to be significantly smaller in comparison with residual tin oxide species and does not depend on the amount of tin in the sample (Fig. 5). The XPS results have been supported by in situ XRD and XANES data of the parent CZA and promoted 1Sn-CZA catalysts.

The in-situ XRD patterns of calcined and reduced catalysts are shown in Fig. 6. The XRD patterns of the calcined catalyst are indicative of the presence of CuO and ZnO oxides over both catalysts without effect of tin on XRD patterns. The size of CuO crystallites calculated using the Scherrer equation was about 8 nm for both samples. The in-situ XRD suggests that CuO reduction into Cu is complete at 290°C with formation of similar Cu crystallites over both catalysts with sizes about 12 nm.

Fig. 7 shows the in-situ Cu K-edge XANES spectra of the non-promoted and tin-promoted samples in comparison with reference materials before and after reduction. CuO sample shows the pre-edge absorption at 8984 eV ascribed to a dipole forbidden transition from 1s to 3d orbital in Cu²⁺ [36]. The oxidized CZA and 1.0Sn-CZA catalysts exhibit XANES spectra similar to that of CuO. However, the pre-edge adsorption over CZA catalysts becomes less obvious in comparison with the reference CuO catalyst. This fact might be explained by smaller sizes of CuO crystallites in CZA catalysts with incorporation of Cu²⁺ into the ZnO-Al₂O₃ framework with different coordination environment and electronic states in comparison with CuO leading to distortion of octahedral coordination [37]. Indeed, TEM analysis of CZA catalyst indicates the high dispersion of Cu in ZnO-Al₂O₃ matrix [38].

Fig. 7b presents the Cu K-edge spectra of in-situ reduced catalysts in comparison with Cu foil. Cu foil shows the absorption edge at 8979 eV and two resonance features at 8993 and 9003 eV. The absorption at the edge at 8979 eV corresponds to 1s to 4p electronic transitions [39]. The

XANES shapes for reduced samples CZA and 1.0Sn-CZA are similar to reference foil indicating the presence of mainly metallic Cu in the sample at the reaction conditions. However, the intensity of edge absorption at 8979 eV over reference copper foil is significantly lower than over CZA and 1.0Sn-CZA. The intensity decreases in the order CZA>1.0Sn-CZA>Cu which can be attributed to the increase in the filling of unoccupied Cu 4p orbital [34]. In the case of CZA sample reduced Cu should be positively charged due to the strong interaction with oxides of ZnO-Al₂O₃ matrix in comparison with the reference Cu foil. The presence of Sn might lead to partial donation of electrons to 4p orbital with decrease of the transition from 1s to 4p.

FTIR spectroscopy yields valuable information about the interaction of Cu surface sites with adsorbed CO. Fig. 8 shows IR spectra measured during CO adsorption at low temperature over CZA and 1.0Sn-CZA catalysts after reduction with increase in CO pressure in the case of reduced catalysts. At low CO coverage (Fig. 8) both samples reveal the most intense band centered at 2120 cm⁻¹. The position of these peaks shifts to 2115 cm⁻¹ with increase in CO pressure. This intense band has been earlier attributed over similar catalyst to the adsorption of CO over Cu⁺ cations or small clusters of metallic copper [40, 41]. This band was very intense over both oxidized catalysts (not shown). Thus, taking also into account high stability of this carbonyl [42] most probably this band might be assigned to Cu⁺-CO species. The shift of the band with increase of CO coverage has been explained by conversion between Cu⁺-CO species and Cu⁺(CO)₂ dicarbonyls [42]. CO adsorption over Cu⁺ species is significantly lower over tin promoted sample. Although, Cu⁺ species have not been observed by “bulk methods” like XRD and XANES, small amounts of Cu⁺ were identified in the catalysts from FTIR analysis of the bands of adsorbed of CO. Further increase in CO coverage leads to appearance of the bands at 2189, 2175 and 2156 cm⁻¹. The first two weak bands correspond to the vibrations of CO adsorbed over Lewis acid sites, Al³⁺ and Zn²⁺, respectively [41]. The band at 2156 cm⁻¹ is typical for the

vibrations of hydrogen bonded CO, in particular, bonded with hydroxyl groups [40]. This is result of CO adsorption over hydroxyl groups of the ZnO-Al₂O₃ matrix and silanol groups of silica which has been used for dissolution of highly absorbing IR light Cu samples. Interestingly, the spectrum of the parent reduced catalyst shows a shoulder at 2135 cm⁻¹ which might be attributed to the presence of more positively charged cationic copper species. The band at 2135 cm⁻¹ has been observed earlier during CO adsorption over Cu⁺ species in ion exchange position of zeolite ZSM-5 [43]. Isolated Cu⁺ species in zeolite should be more positively charged in comparison with Cu⁺ stabilized by ZnO-Al₂O₃ matrix. Note that this feature is absent in the FTIR spectra of CO adsorbed over the promoted catalysts.

To conclude, promotion of the CZA catalyst by tin leads to modification of the properties of both cationic and metallic copper species. Tin promotion leads to the decrease of ionic copper fraction (Cu⁺ and Cu²⁺) in the reduced catalysts due to the strong interaction between copper and tin in the catalyst. At the same time, tin inhibits reduction of copper, decreases the surface area of metallic copper probably by formation Cu-Sn alloys and increases the electronic density on the metal.

3.2 DME synthesis and WGS paths in the unpromoted and tin-promoted catalysts

The catalytic activities and selectivities in DME synthesis of the composite CZA/HZSM-5 and Sn-CZA/HZSM-5 catalysts are shown in Figs. 9-12. The carbon monoxide conversions and selectivities are strongly affected by the presence of tin in CZA. The conversion decreases as a function of tin content in the catalysts and follows the following order (Fig. 9): CZA/HZSM-5 \approx 0.1Sn-CZA/HZSM-5 > 0.2Sn-CZA/HZSM-5 > 0.5Sn-CZA/HZSM-5 > 1.0Sn-CZA/HZSM-5.

The observed phenomena might be explained by the lower activity of the formed Cu-Sn nanoparticles containing tin species in comparison with copper species in the parent CZA (Table 1). The decrease in the activity of the noble metals after doping by tin has been explained earlier

by blocking of the surface sites by ligand effect and electronic effects [35]. The effect of change of catalytic performance during hydrogenation/dehydrogenation reactions by tin promotion has been explained by several authors by electronic interaction between tin and metal [44-45]. In the case of Pt the influence of tin as promoter has been assigned to donation of electrons to 5d band leading to deactivation of the active sites [44]. In the case of copper it should result in decrease of the participation of 3d electrons in bonding with exclusion of these sites from interaction with CO. The effect of tin as deactivating agent with inhibition of hydrogenolysis has been found to be similar to deactivation by coke deposition [45]. In both cases coke and tin selectively deactivated unselective Pt sites.

It is interesting to note (Fig. 9) that small amount of added Sn (0.1 %) almost does not affect the activity of the catalyst while the tin amount higher than 0.2 wt. % significantly reduces the catalytic activity. It indicates that Cu sites in the parent CZA samples might be not uniform. Indeed, FTIR spectra of adsorbed CO over in situ reduced CZA catalysts (Fig. 8) indicated the presence of Cu^+ species in addition to copper metallic phase observed by in situ XRD (Fig. 6) and XANES (Fig. 7).

DME is the main product of the reaction with the selectivity in the range of 68-76 % (Fig. 10). The selectivity to methanol varies from 3 to 6 %. Methanol is the primary reaction product of DME synthesis. As expected for primary products, highest methanol selectivity is observed at low carbon monoxide conversions. Light hydrocarbons are produced with low selectivities (0.1-2 %). All the catalysts showed very significant selectivity to CO_2 which increases with carbon monoxide conversion. Carbon dioxide forms in WGS. The ratio of DME to CO_2 selectivities over parent catalyst (2.3:1) is higher than the theoretical ratio of 2:1. This suggests that part of water produced via methanol dehydration during DME synthesis does not participate in WGS reaction.

Higher tin content in the CZA catalyst results in the gradual increase in the selectivity to DME from 68 % over the parent CZA/ZSM-5 catalyst to 76 % over the tin promoted catalyst. Taking into account methanol, the combined selectivity to DME and methanol increases from 71 to 80 %. This effect is mainly the result of lower CO₂ selectivity which decreases from 28 to 18 %. The variation of the selectivity might be explained both by lower CO conversion in the tin-promoted catalysts and by the effect of tin on WGSR.

Tin was introduced by impregnation of the CZA catalyst. We assume that tin introduction selectively affects only the CZA catalyst. In order to further clarify the effect of tin on the DME selectivity, the tests have been conducted over the parent CZA/ZSM-5 catalytic systems with lower CZA content to simulate the lower activity of tin promoted Sn-CZA/ZSM-5. Fig. 10 shows conversion of CO and selectivities over CZA/ZSM-5 with the ratio CZA/ZSM-5 in the catalyst equal to 5/3, 1/1 and 1/2. The conversion of CO decreases from 69.2 to 51.3 and 29.3 % as a function of CZA content in the bifunctional catalyst. Lower CO conversion coincides with the increase in DME selectivity from 68.3 to 69.6 and 70.4 %, respectively. Lower carbon monoxide conversion results in the lower CO₂ selectivity similar to the tin promoted samples and might be explained by lower amounts of produced water in the system. Interestingly lower carbon dioxide and higher DME selectivities were observed at the similar conversions over the tin promoted catalysts compared to the parent catalyst (Figs. 10 and 11). Indeed, at the conversion of about 29 % over 0.5Sn-CZA/ZSM-5 and CZA/ZSM-5=1/2 the selectivity to DME is 6 % higher over the tin promoted catalyst. The selectivity to CO₂ is lower by approximately 5 % over promoted systems in comparison with parent catalyst at the same conversions (Fig. 11). In the case of mild promotion (0.1 and 0.2 wt. % Sn) higher methanol selectivity is also observed which might be explained by higher water content in the reactor with its significant adsorption over acid sites of ZSM-5 which explains lower activity in dehydration of methanol to DME. The selectivity

to hydrocarbons has been also slightly increased with higher amount of tin. This effect is due to the lower conversion of CO and might be observed also over CZA/ZSM-5 with higher zeolite fraction in the catalyst (Fig. 10).

One of the possible explanations of these observations can be related to the selective effect of tin addition on WGS in comparison with CO hydrogenation to methanol. The most interesting effect in terms of the catalyst selectivity is observed over mildly promoted CZA catalysts (0.1Sn-CZA). Indeed, almost at the same conversion of CO the combined selectivity to DME and methanol increases from 71 to 76 %.

Higher CO₂ and lower DME selectivities in the parent CZA/HZSM-5 catalyst might be explained by the presence of the sites in the CZA catalyst more active in WGS reaction in comparison with tin-promoted catalysts. Probably these are the Cu^{δ+} sites more positively charged in ZnO-Al₂O₃ matrix shown by FTIR (Fig. 8). Earlier investigations of the WGS reaction over Cu catalysts doped by oxides (ZrO₂, CeO₂) have shown that Cu sites interacting with O vacancy with easy redox Cu²⁺ to Cu⁺ pairs are responsible for high WGS activity [46,47]. The presence of tin might result in the preferably reduction of these Cu⁺ sites with formation of Cu-Sn alloy with increase of the selectivity to DME. This assumption is supported by the fact that the selectivity to CO₂ over promoted catalysts is always lower by 5 % in the whole conversion range in comparison with the unpromoted system (Fig. 11). This means that deactivation of most part of unselective sites take place already at low amount of added tin. Further increase in the amount of tin leads to the decrease in the fraction of the active surface metallic Cu and lower reaction rate in carbon monoxide hydrogenation (Table 1). To provide further insights into the effect of tin, the transformation of CO in the presence of water has been studied over the promoted catalysts. Fig. 12 shows CO conversion of versus tin content in the CZA catalysts. The main reaction products were CO₂ and H₂. The conversion of CO significantly decreases with the increase in Sn content.

The presence of 0.1 wt. % of Sn results already in decrease in the conversion of CO from 71 to 60 %. The conversion drops to 23 % at higher tin content. Thus, indeed, the effect of tin over the CZA catalyst might be explained by lower rate of the WGS reaction. Small amounts of tin introduced to the CZA catalyst can principally deactivate the sites active in WGS reaction. Consequently lower CO₂ and higher DME selectivities are observed on the tin-promoted catalysts.

Most of previous research in the field of DME synthesis has addressed the catalyst promotion in order to decrease hydrocarbon selectivity. For example, promotion of zeolite by metal oxides (ZrO₂, MgO) resulted in increase in the selectivity to DME mainly due to suppression of hydrocarbons formation [48, 49]. The maximal selectivity to DME at the similar reaction conditions over CZA/ZSM-5 catalyst promoted by MgO was 64.5 % [48]. The neutralization of external acid sites of ZSM-5 performed in [38] significantly increased the stability of the catalyst with only slight increase of the selectivity to 69 % due to higher hydrophobicity of the catalyst and lower holdup of the water in the system. Application of zeolite-CZA capsule catalyst exhibited very high selectivity to DME due to suppression of further dehydration of DME to form alkane/alkene byproducts, although the activity of the composite catalyst was very low [50]. It seems important to emphasize however those hydrocarbons are not the main side reaction products of carbon monoxide hydrogenation over bifunctional copper-zeolite catalysts with mild acidity. CO₂ is a major undesirable product which significantly reduces the carbon efficiency of the direct DME synthesis. Modification of the Cu based catalyst with tin provides new opportunities to increase the selectivity to DME by suppression of WGS.

4. Conclusion

The structure of copper species in Cu-Zn-Al catalyst has been shown to be significantly affected by the presence of tin as a promoter. TPR, XPS, in-situ XRD, in-situ XANES and FTIR

measurements reveal the presence of the tin in reduced state and the presence of positively charged Cu^+ copper species in the parent catalyst. The presence of these copper species were indicated by FTIR.

The catalytic performance in direct DME synthesis from syngas of hybrid CuZnAl/ZSM-5 prepared by grinding depends on the amount of tin. An increase in the amount of the promoter results in the decrease in the catalyst activity which is accompanied by the increase of the DME selectivity. The presence of tin suppresses the WGS reaction and consequently reduces CO_2 production. The optimum amount of tin in the catalyst has been found to be 0.1 wt.%. At this tin content, almost no effect on the carbon monoxide hydrogenation rate was observed and the combined selectivity to DME and methanol increased by 5 % relative to the unpromoted catalyst.

5. Acknowledgments

This research is being performed within the ANR project CATSYN-BIOFUELS (ANR-12-BS07-0029). The authors gratefully acknowledge the support of the French National Research Agency. The authors gratefully acknowledge technical support from SNBL. The ESRF is acknowledged for use of synchrotron radiation. The authors would like to thank Dr. Wouter Van Beek (SNBL/ESRF) for technical assistance

5.

References

1. A. Corma, S. Iborra, A. Vely, Chem. Rev. 107 (6) (2007) 2411-2502.
2. T. Fleisch, E. Iglesia, J. Spivey, Natural Gas Conversion VI, Vol. 136, Elsevier, 2001.
3. S. Lee, Methanol synthesis technology, CRC Press, 1989.
4. J. Rezaian, N. P. Cheremisinoff, Gasification technologies: a primer for engineers and scientists, CRC press, 2005.

5. K. Liu, C. Song, V. Subramani, Hydrogen and syngas production and purification technologies, Wiley Online Library, 2010.
6. Q. Ge, Y. Huang, F. Qiu, S. Li, Appl. Catal. A 167 (1) (1998) 23-30.
7. T. A. Semelsberger, R. L. Borup, H. L. Greene, J. Power Sources 156 (2) (2006) 497-511.
8. C. Arcoumanis, C. Bae, R. Crookes, E. Kinoshita, Fuel 87 (7) (2008) 1014-1030.
9. F. Yaripour, F. Baghaei, I. Schmidt, J. Perregaard, Catal. Commun. 6 (2) (2005) 147-152.
10. S. Jiang, J.-S. Hwang, T. Jin, T. Cai, W. Cho, Y.S. Baek, S.E. Park, Bull. Korean Chem. Soc. 25 (2) (2004) 185-189.
11. S.-M. Kim, Y.J. Lee, J. W. Bae, H. Potdar, K.-W. Jun, Appl. Catal. A 348 (1) (2008) 113-120.
12. K. Sun, W. Lu, F. Qiu, S. Liu, X. Xu, Appl. Catal. A 252 (2) (2003) 243-249.
13. Y. Amenomiya, Appl. Catal. A 30 (1) (1987) 57-68.
14. C. Jiang, D. Trimm, M. Wainwright, N. Cant, Appl. Catal. A 93 (2) (1993) 245-255.
15. F. Ramos, A. Farias, L. E. P. Borges, J. Monteiro, M. A. Fraga, E. F. Sousa-Aguiar, L. G. Appel, Catal. Today 101 (1) (2005) 39-44.
16. T. Takeguchi, K.-I. Yanagisawa, T. Inui, M. Inoue, Appl. Catal. A 192 (2) (2000) 201-209.
17. K. S. Yoo, J.-H. Kim, M.-J. Park, S.-J. Kim, O.-S. Joo, K.-D. Jung, Appl. Catal. A 330 (2007) 57-62.
18. K. Sun, W. Lu, F. Qiu, S. Liu, X. Xu, Appl. Catal. A 252 (2003) 243-249.
19. Z. Li, J. Li, Ch. Yang, J. Wu, J. Natur. Chem. 21 (2012) 360-365.
20. X.-J. Tang, J.-H. Fei, Zh.-Y. Hou, X.-M. Zheng, H. Lou, Energ. Fuel 22 (2008) 2877-2884.
21. J.-H. Fei, X.-J. Tang, Zh.-Y. Huo, H. Lou, X.-M. Zheng, Catal. Comm. 7 (2006) 827-831.

22. M. Toba, S.-I. Tanaka, S.-I. Niwa, F. Mizukami, Z. Koppány, L. Guzzi, K.-Y. Cheah, T.-S. Tang, *Appl. Catal. A* 2 (189) 243-250.
23. R. Gavagnin, L. Biasetto, F. Pinna, G. Strukul, *Appl. Catal. A* 38 (2002) 91-99.
24. S. Galvagno, Z. Poltarzewski, A. Donato, G. Neri, R. Pietropaolo, *J. Mol. Catal.* 35 (1986) 365-373.
25. J.B. Ko, C.M. Bae, Y.S. Jung, D.H. Kim, *Catal. Lett.* 105 (2005) 157-161.
26. W.R.A.M. Robinson, J.C. Mol, *Appl. Catal.* 60 (1990) 73-86.
27. M. Rønning, N.E. Tsakoumis, A. Voronov, R.E. Johnsen, P. Norby, W. van Beek, Ø. Borg, E. Rytter, A. Holmen, *Catal. Today* 155 (2010) 289-295.
28. H. Karaca, J. Hong, P. Fongarland, P. Roussel, A. Griboval-Constant, M. Lacroix, K. Hortmann, O.V. Safonova, A.Y. Khodakov, *Chem. Commun.* 46 (2010) 788-790.
29. P.D. Zgolicz, V.I. Rodríguez, I.M.J. Vilella, S.R. de Miguel, O.A. Scelza, *Appl. Catal. A* 392 (2011) 208-217.
30. W.L. Dai, Q. Sun, J.F. Deng, D. Wu, Y.H. Sun, *Appl. Surf. Sci.* 177 (2001) 172-179.
31. P.H. Matter, D.J. Braden, U.S. Ozkan, *J. Catal.* 223 (2004) 340-351.
32. L. Alejo, R. Lago, M.A. Pena, J.L.G. Fierro, *Appl. Catal. A* 162 (1997) 281-297.
33. R. T. Figueiredo, A. Martinez-Arias, M. Lopez Granados, J. L. G. Fierro, *J. Catal.* 178 (1998) 146-152.
34. J.H. Kim, S.M. Choi, S.H. Nam, M.H. Seo, S.H. Choi, W.B. Kim, *Appl. Catal. B* 82 (2008) 89-102.
35. F. Coloma, A. Sepulveda-Escribano, J.L.G. Fierro, F. Rodriguez-Reinoso, *Appl. Catal. A* 148 (1996) 63-80.
36. E.B. Fox, S. Velu, M.H. Engelhard, Y.H. Chin, J.T. Miller, J. Kropf, C. S. Song, *J. Catal.* 260 (2008) 358-370.

37. D. Gamarra, G. Munuera, A.B. Hungria, M. Fernandez-Garcia, J.C. Conesa, P. A. Midgley, X. Q. Wang, J. C. Hanson, J. A. Rodriguez, A. Martinez-Arias, *J. Phys. Chem. C* 111 (2007) 11026-11038.
38. V.V. Ordonsky, M. Cai, V. Sushkevich, S. Moldovan, O. Ersen, C. Lancelot, V. Valtchev, A.Y. Khodakov, *Appl. Catal. A* 486 (2014) 266-275.
39. Z. Sun, M. Meng, L. Zhang, Y. Zha, X. Zhou, Z. Jiang, S. Zhang, Y. Huang, *Int. J. Hydrogen Energy* 37 (2012) 18860-18869.
40. K.I. Hadjiivanov, G.N. Vayssilov, *Adv. Catal.* 47 (2002) 307-511.
41. G. Busca, U. Costantino, F. Marmottini, T. Montanari, P. Patrono, F. Pinzari, G. Ramis, *Appl. Catal. A.*, 310 (2006) 70-78.
42. K. Hadjiivanov, T. Tsoncheva, M. Dimitrov, C. Minchev, H. Knözinger, *Appl. Catal. A* 241 (2003) 331.
43. J. Szanyi, M.T. Paffett, *J. Chem. Soc., Faraday Trans.* 92(24) (1996) 5165-5175.
44. G. Cocco, S. Enzo, *J. Chem. Soc., Faraday Trans* 81 (1985) 321.
45. J. Völter, U. Kürschner, *Appl. Catal.* 8 (1983) 167.
46. J.B. Ko, C.M. Bae, Y.S. Jung, D.H. Kim, *Catal. Lett.* 105 (2005) 157-161.
47. K. Nishida, D. Li, Y. Zhan, T. Shishido, Y. Oumi, T. Sano, K. Takehira, *Appl. Clay Sci.* 44 (2009) 211-217.
48. M. Dongsen, Y. Weimin, X. Jianchao, Zh. Bin, S. Qingying, Ch. Qingling, *J. Catal.* 230 (2005) 140-149.
49. S.-H. Kang, J.W. Bae, K.-W. Jun, H.S. Potdar, *Catal. Commun.* 9 (2008) 2035-2039.
50. G. Yang, N. Tsubaki, J. Shamoto, Y. Yoneyama, Y. Zhang, *JACS* 132 (2010) 8129-8136.

Table 1.
Characterization of CZA

Sample	TPR results		XPS analysis Cu 2p 3/2		Cu surface area and dispersion (N ₂ O decomposition)	
	T reduction, °C	H ₂ consumption (mmol H ₂ /g _{cat})	Position, eV	Area	S, m ² /g _{cat}	D, %
CZA	264	6.9	932.8	5572.3	36.2	12.2
0.1Sn-CZA	265	5.0	932.5	5149.5	31.2	14.5
0.5Sn-CZA	273	4.7	932.5	5004.4	24.5	12.0
1.0Sn-CZA	280	4.3	932.4	4817.2	18.9	10.2

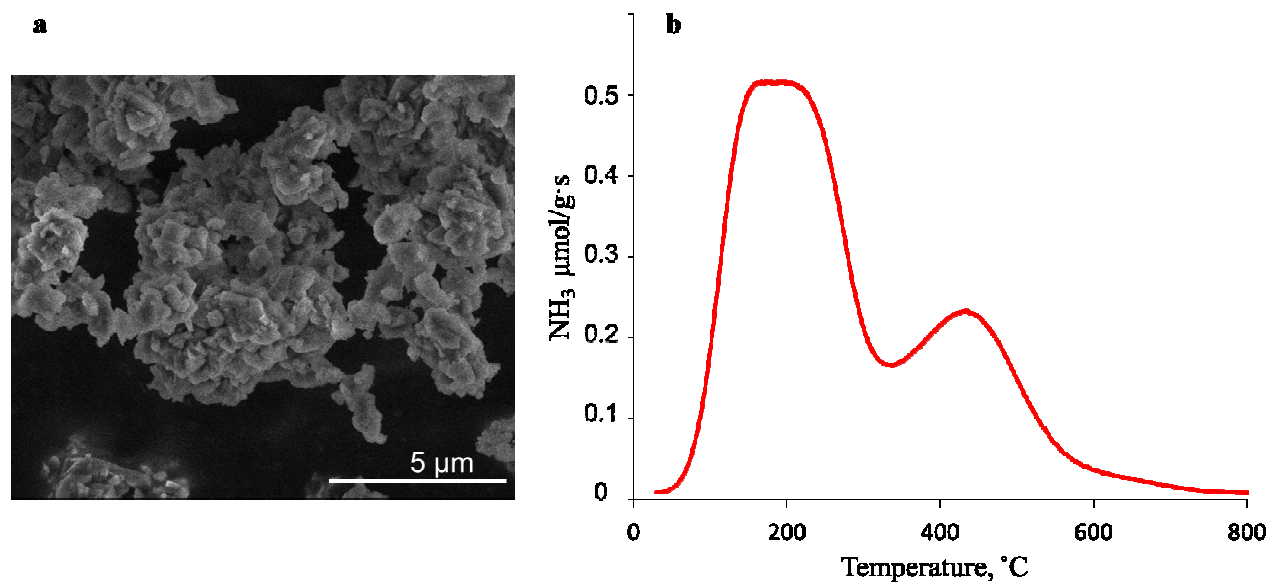


Fig. 1. SEM micrographs of ZSM-5 (a) and TPD NH₃ profiles for zeolite ZSM-5

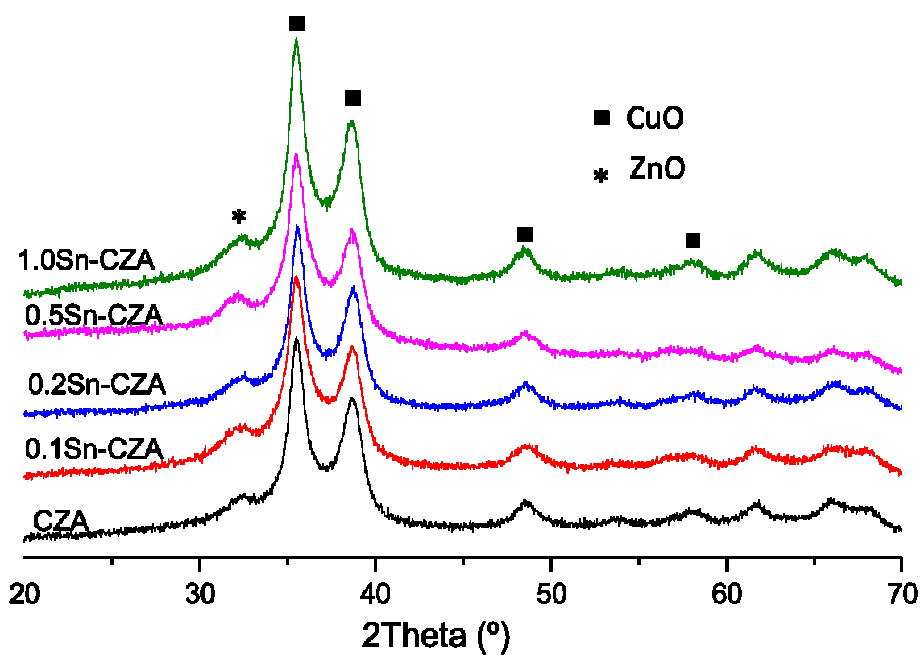


Fig. 2. XRD patterns of the parent and Sn promoted CuO-ZnO-Al₂O₃ catalysts

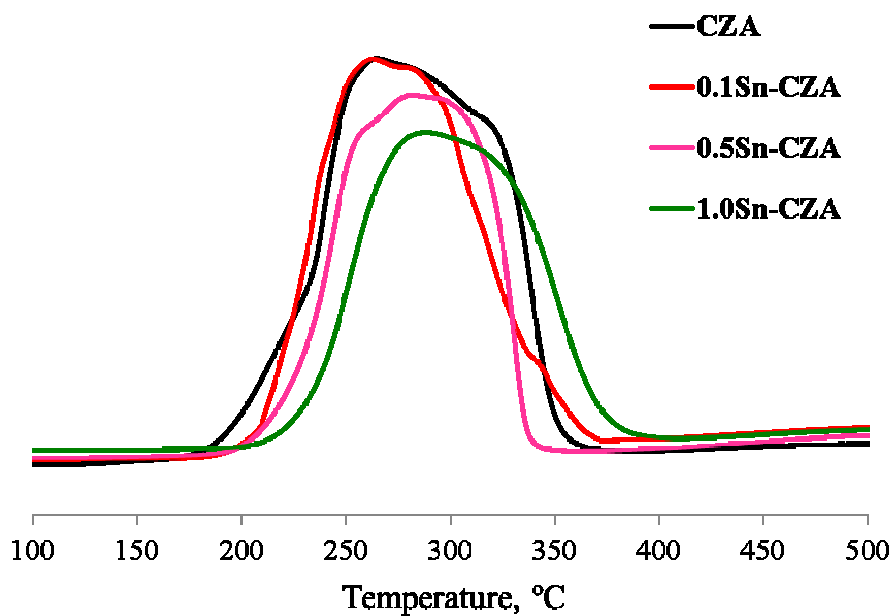


Fig. 3. TPR patterns of the parent and Sn promoted CuO-ZnO-Al₂O₃ catalysts

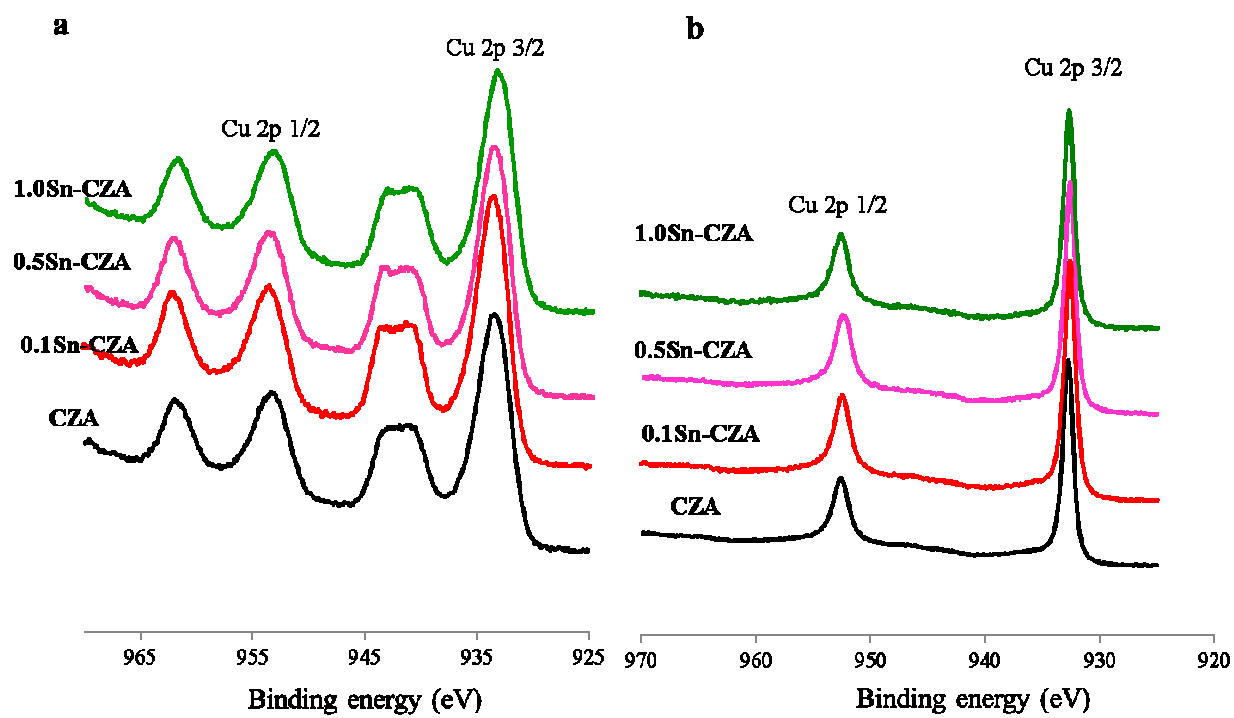


Fig. 4. XPS spectra (Cu 2p region) of the parent and Sn promoted CuO-ZnO-Al₂O₃ catalysts before (a) and after reduction (b)

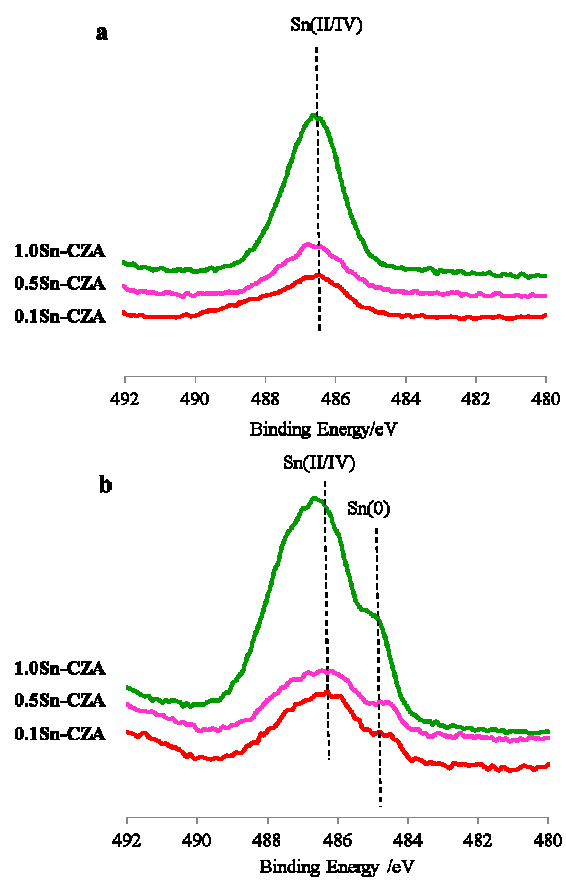


Fig. 5. XPS spectra (Sn 3d_{5/2} region) of the Sn promoted CuO-ZnO-Al₂O₃ catalysts before (a) and after reduction (b)

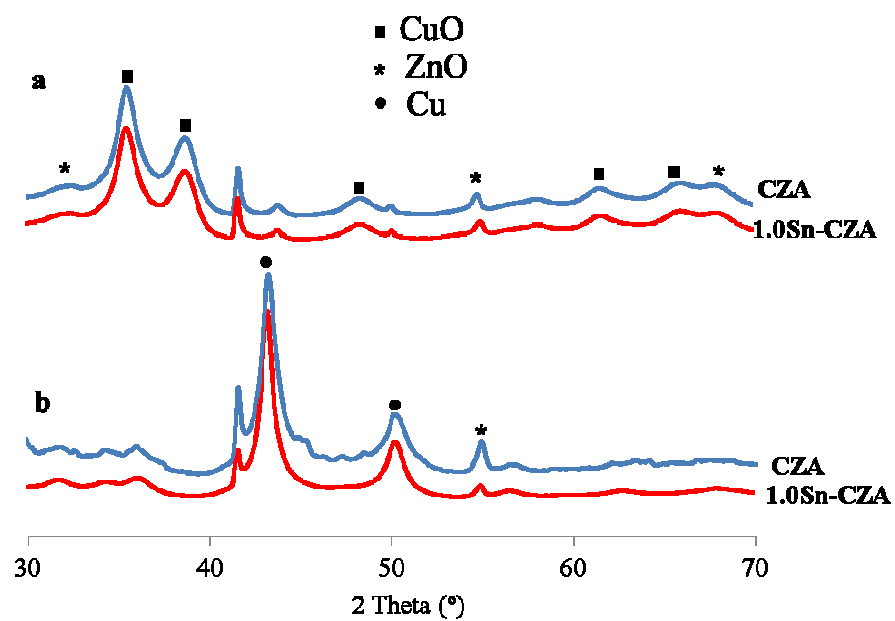


Fig. 6. In situ XRD patterns of CZA or 1.0Sn-CZA measured at before (a) and after (b) reduction in hydrogen

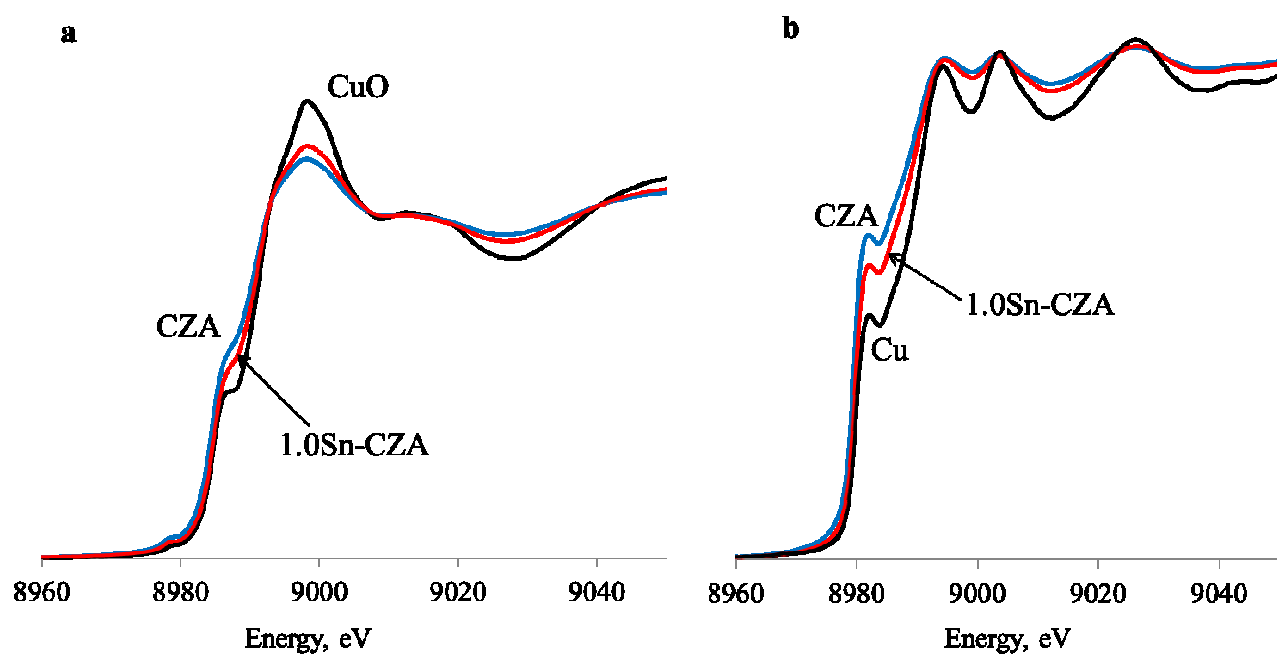


Fig. 7. In situ XANES spectra of catalysts CZA and 1.0Sn-CZA before (a) and after reduction (b) in hydrogen in comparison with CuO and Cu foil reference compounds

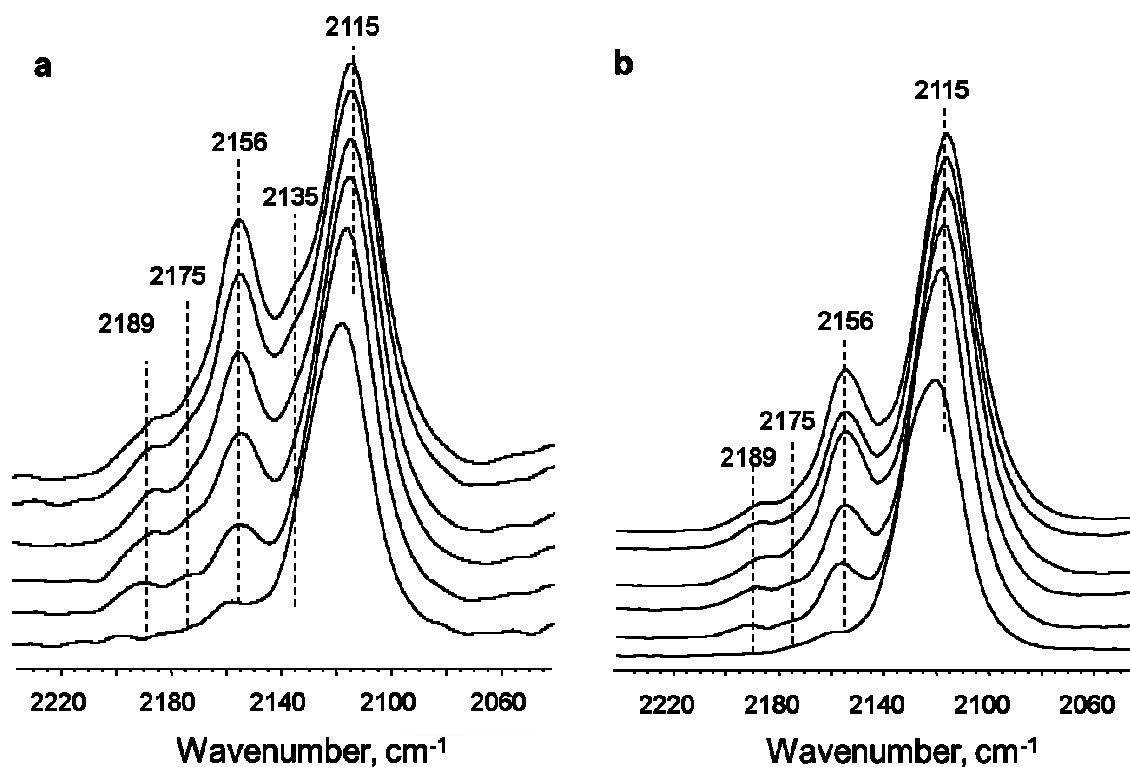


Fig. 8. FTIR spectra of low temperature CO adsorption over parent (a) and Sn promoted catalyst 1.0Sn-CZA (b)

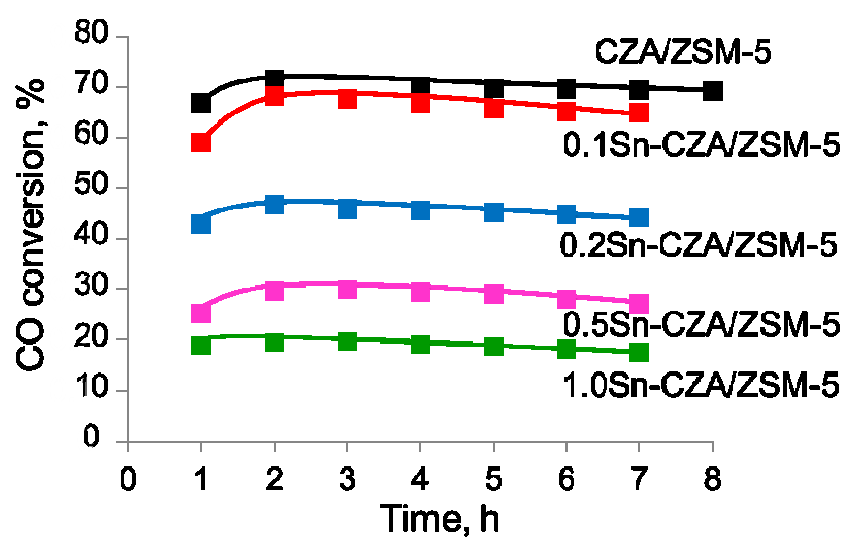


Fig. 9. CO conversion in time during DME synthesis over hybrid catalysts CZA/zeolite with parent CZA and promoted by Sn

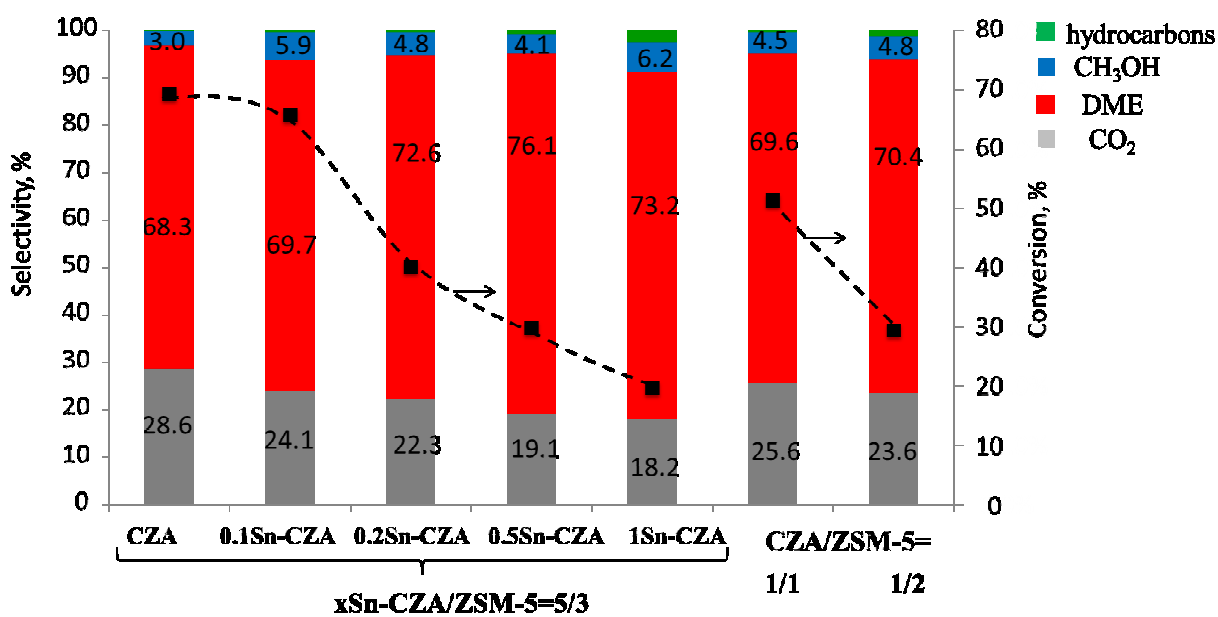


Fig. 10. Selectivity to main products during DME synthesis over hybrid catalyst CZA/zeolite with parent CZA and promoted by Sn with the weight ratio CZA to ZSM-5 equal to 5/3 and CZA to ZSM-5 equal to 1/1 and 1/2

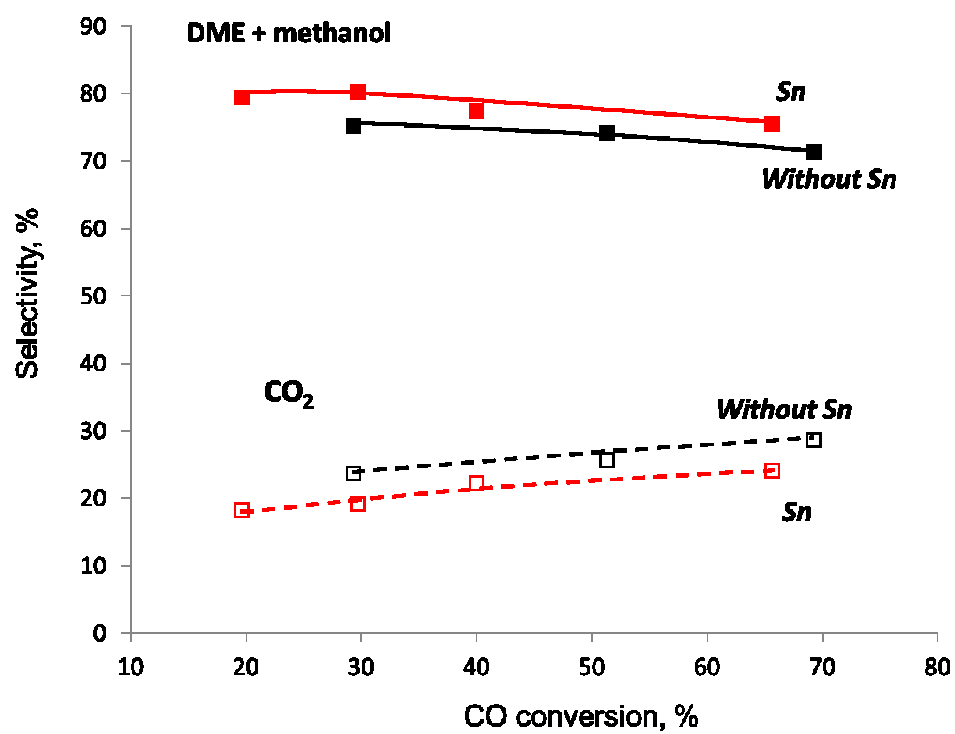


Fig. 11. Selectivity to DME+methanol and CO₂ over parent and tin promoted hybrid catalyst CZA/zeolite

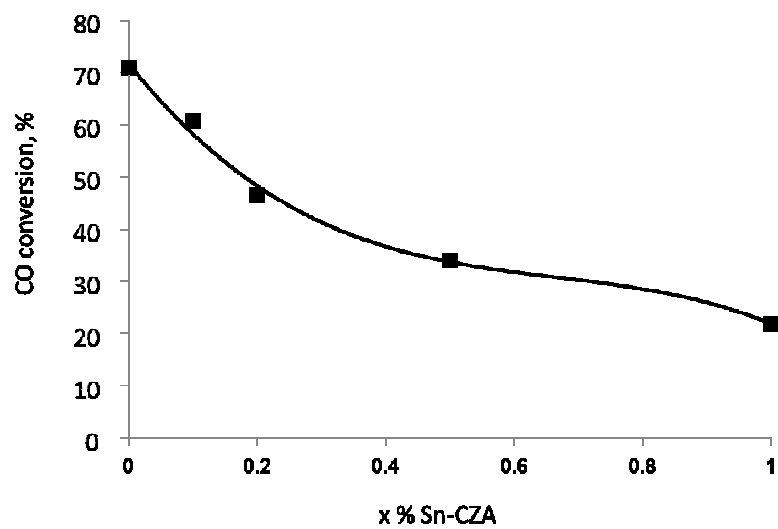


Fig. 12. CO conversion during WGS reaction depending on the Sn content in CZA catalyst